Step and flash imprint lithography template characterization, from an etch perspective

W. J. Dauksher,[a] D. P. Mancini, K. J. Nordquist, D. J. Resnick, D. L. Standfast, D. Convey, and Y. Wei
Motorola Labs, Microelectronics and Physical Sciences Laboratory, Tempe, Arizona 85284

(Received 8 July 2003; accepted 6 October 2003; published 5 December 2003)

As a means of studying process windows with short turnaround time while avoiding substrate-to-substrate repeatability issues, Step and Flash Imprint Lithography templates were fabricated with physical masking of quadrants during dry etching used to introduce process perturbations. For every 20 s of descum (Ar/O_2 etch) time, critical dimensions (CD) were observed to change approximately 2.6 nm on sub-100 nm features. Similarly, increasing Cr overetch time by 20% resulted in a positive CD change of 3.8 nm. Line edge roughness decreased with increasing descum and Cr overetch times. Best overall performance was observed for a 20 s descum used in conjunction with a 110% Cr overetch. Of four tip types studied, sharpened silicon atomic force microscopy tips were able to accurately measure etch depth of 80 nm trenches, but geometrical considerations limited sidewall angle determination to greater than 100°. Cross-sectioning of features on $6 \times 6 \times 0.25$ in. quartz plates was successfully accomplished using a focused ion beam technique with typical sidewall angles of about 95° observed on 150 nm features. Finally, minimal microloading was observed for the ICP-based quartz etch process. Feature sizes ranging from 70 nm up to 8 μm possessed an average etch depth of 88.8 nm with a 1.2 nm (1 sigma) variation. © *2003 American Vacuum Society.* [DOI: 10.1116/1.1629299]

I. INTRODUCTION

Step and flash imprint lithography (SFIL) has recently garnered a significant amount of attention because of the potential to fabricate lower margin devices such as filters, waveguides, and photonic crystals at a reduced cost of ownership as compared to other next generation lithographies. Very briefly, SFIL entails the use of a quartz template with relief[1,2] that is pressed with low force into a low viscosity organosilicon layer. The organosilicon layer is photosensitive, and exposure through the template to either broadband illumination or radiation of a certain wavelength results in crosslinking of the organosilicon monomers. The resulting imprinted image becomes the basis of the mask used to pattern transfer a film on the substrate.

From an etch perspective, various attributes of the template such as critical dimension (CD) control, minimization of microloading effects (etch rate dependency on local pattern density), and feature profile are essential to successfully enact SFIL technology. In this article, these attributes will be discussed extensively as they relate to SFIL templates fabricated by using a thin Cr hardmask.

For the purpose of studying processing changes without introducing substrate-to-substrate repeatability questions, SFIL templates were written with a replicating dose array present in each of four quadrants on a $6 \times 6 \times 0.25$ in. (6025) quartz plate. Each of the quadrants was physically masked during a specific etch process to study perturbations. Illustrative results from an Ar/O_2 descum and a chlorine-based chrome etch process will be presented. Such extensive characterization is invaluable in that it provides not only a path to optimizing CD bias[3] but also allows for flexibility in tailoring other attributes, such as resist thickness.

An elaborate atomic force microscopy (AFM) study was conducted as a means of ascertaining quartz etch depth and feature sidewall angle. Of course, ultimate verification of sidewall angle may be obtained via the imprinting process itself, but AFM affords an opportunity for nondestructively qualifying both etch depth variations (i.e., microloading) and, to a lesser degree, sidewall angle on SFIL templates. The results of a study comparing standard, carbon nanotube, high aspect ratio, and sharpened silicon AFM tips will be outlined. The geometrical limitations of AFM will briefly be discussed, and corroborating cross-sectional results from specially prepared 6025 plates shown.

II. EXPERIMENTAL METHODS

For the fabrication of templates, 15 nm Cr was sputtered on to standard 6025 plates. ZEP520A resist spun to a nominal thickness of 160 nm was imaged on a Leica VB-6 HR electron beam exposure system operating at 100 kV. As depicted in Fig. 1, patterning was done in the center 25×25 mm^2 of each of four quadrants on the 6025 plates. In turn, within each quadrant, four resolution test patterns were written at four doses ranging from 700 to 1000 $\mu C/cm^2$.

Pattern transfer was performed in a partially customized Plasma Therm VLR tool adapted to accommodate 6025 plates. To maximize cycles of learning and to minimize plate-to-plate variation, physical masking was employed during some of the etches in order to process each of the four quadrants on a template with four different time splits or conditions. The masking was accomplished by placing square silicon pieces over quadrants of the templates. On any

[a]Electronic mail: axyx50@motorola.com

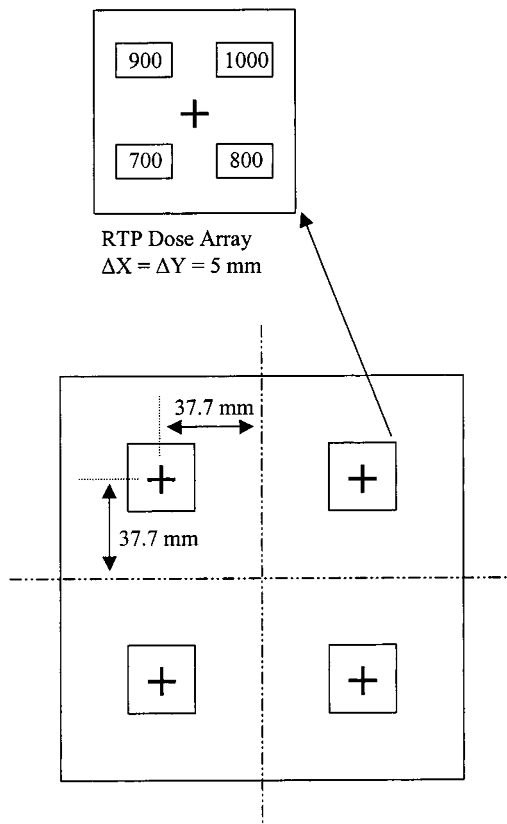

FIG. 1. Schematic diagram showing the layout of the four quadrant arrays written on 6025 plates for etch splits. Each quadrant contained a dose array of resolution test patterns.

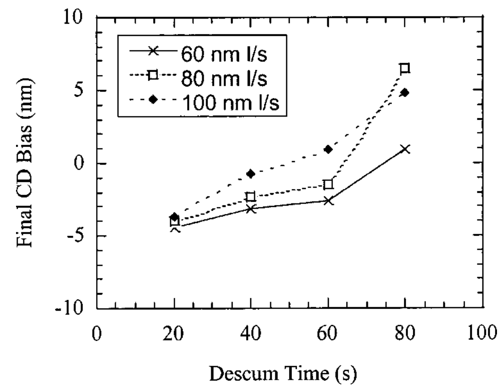

FIG. 2. Final CD bias on a completed SFIL template as a function of descum time. The template saw a 60% Cr overetch.

given substrate, only one such masking etch split was employed (e.g., a descum split) while all of the other etches in the fabrication sequence were kept as the baseline processes of record.

One of the etch processes studied via masking splits was the descum process. The fundamentals of the Ar/O_2 etch, modified in the present work to emulate wafer performance on plates, has been previously described in the literature.[4] Very briefly, the vertical to horizontal etch rate ratio is greater than 9:1 which minimizes CD bias of the process while effectively removing any resist scum and trimming profiles. Time splits of 20, 40, 60, and 80 s were conducted on templates.

The other etch process in which masking splits were studied was the Cr hardmask etch. Once again, the basis for the RIE Cr etch process on 6025 plates was an extension of a well-characterized wafer process.[5] Endpoint during the chrome pattern transfer step was determined by monitoring the optical emission signal of a chlorine line. Since the chrome overetch must be at least 60% to obtain vertical sidewalls, overetch splits of 60%, 80%, 100%, and 120% were run at 75 W rf. After performing the Cr etch, the resist was stripped in a piranha solution ($4\,H_2SO_4:1\,H_2O_2$) operating at 105 °C.

An inductively coupled plasma (ICP) process was developed and optimized for performing the quartz etch on SFIL templates. Because of the high selectivity of quartz to chrome in the process, only a thin Cr layer was required as a hardmask. This fluorine-based process is run at a pressure of 5 mT and was used to etch to a target depth of 100 nm into the quartz templates. After quartz pattern transfer, the remaining Cr hardmask layer was stripped using a commercially available ceric ammonium nitrate solution.

Comprehensive CD data was collected at six stages of processing of the templates: after e-beam writing; descum; Cr etch; resist strip; quartz etch; and Cr hardmask removal. Dense and semidense features 100 nm and below in size comprised the data set collected. Both the CD data and top-down complementary images of features were taken using an S-7800 CD scanning electron microscope (SEM) manufactured by Hitachi.

Finally, additional characterization was undertaken on some of the templates. Etch depth and, to a lesser degree, sidewall angle information were obtained using a Digital Instruments DM3000 Scanning Probe Microscope (AFM). The quartz features were imaged using standard, carbon nanotube, high aspect ratio, and sharpened silicon AFM tips. A successful technique for cross-sectioning the quartz trenches and subsequently imaging via SEM was found by using an FEI 835 focused ion beam (FIB) tool.

III. CRITICAL DIMENSION RESULTS

A. Descum process

Using the baseline descum process, the etch rate of resist on 6025 plates was found to be about 37 nm/min. Predicated on this information, time splits of 20, 40, 60, and 80 s were chosen; the maximum theoretical resist loss for the longest run was calculated to be 49.3 nm. Figure 2 contains a plot of final CD bias from coded as a function of descum time for intervals of 20 to 80 s. The data is plotted for three clustered line/space sizes: 60; 80; and 100 nm. To a first approximation, a slight positive slope of about 2.6 nm CD change (spaces increase in size) exists per 20 s of descum time. As an interesting side note, the data appears to spread out with descum time such that the larger trenches grow more as compared to the smaller trenches. One possible etch-related explanation for this behavior is that gas phase transport of reactive species is easier given larger feature sizes.

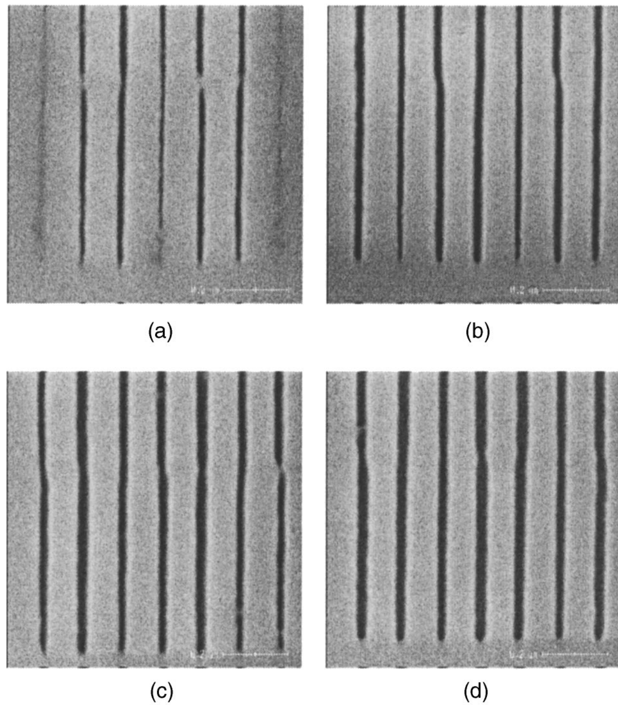

FIG. 3. SEM images of 30 nm spaces/90 nm lines on a completed SFIL template. CD measurements are: (a) 16.9 nm; (b) 23.1 nm; (c) 25.5 nm; and (d) 29.6 nm for process splits of 20, 40, 60, and 80 s descum. A 60% Cr overetch was used.

Figure 3 shows SEM images of 30 nm spaces/90 nm lines on a completed SFIL template as a function of descum time. Although an e-beam writing error and other effects are present in the images, the results of increasing descum time are obvious. The 30 nm features that received the shortest descum time of 20 s are only partially cleared out; increasing descum time produces crisper features with a concomitant increase in critical dimension.

B. Cr etch process

Complementary etch development work was also undertaken on the chlorine-based chrome hardmask process. The optimized RIE etch process at 75 W has a chrome etch rate of 7.5 nm/min, an average chrome to resist selectivity of 0.45:1, and a chrome uniformity $[(\max-\min)/(2^{\star}\text{mean})]$ of 6.6%. The Cr splits were selected so as to vary overetch time from 60% (minimum necessary for a straight sidewall) to 120% (maximum permissible resist loss of about 75 nm). Plotted in Fig. 4 is final CD bias from coded feature size as a function of chrome overetch. All results shown are for 80 nm features. The data is comprised of information from three templates, one each receiving a descum of 20, 40, and 60 s.

Similar to observations made for increasing descum time, a positive CD change of 3.8 nm per 20% of Cr overetch exists. As would be expected, the CD bias from coded for a given Cr overetch percentage becomes more positive with increasing descum time. Clearly, both Cr overetch percentage and resist descum have a big and well-defined impact on final critical dimensions. By generating a plot similar to that

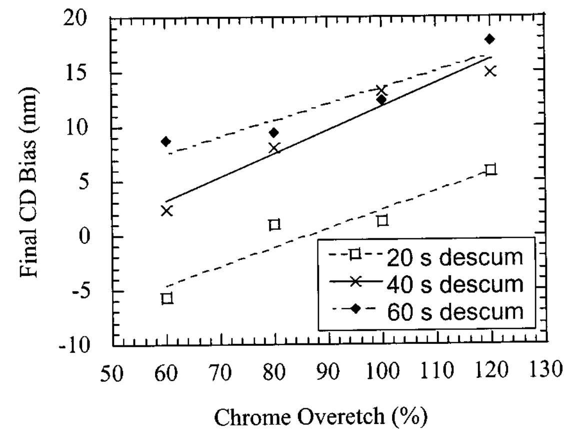

FIG. 4. Final CD bias on three completed SFIL templates as a function of chrome overetch. The three templates were given descums of 20, 40, and 60 s. The CD measurements were taken on 80 nm features.

shown in Fig. 4 for all feature sizes of interest and then superimposing acceptable CD variation limits (e.g., ±10%), a process window can be defined.

The complementary figure to Fig. 3 may be found in Fig. 5. Here, SEM images of 40 nm spaces/80 nm lines are shown for a completed SFIL template. For the Cr etch process splits, CD measurements were observed to increase from 32.4 to 39.7 nm as overetch increased from 60% to 120%. Line edge roughness was in general excellent for all splits, but it did subtly improve with increasing chrome overetch.

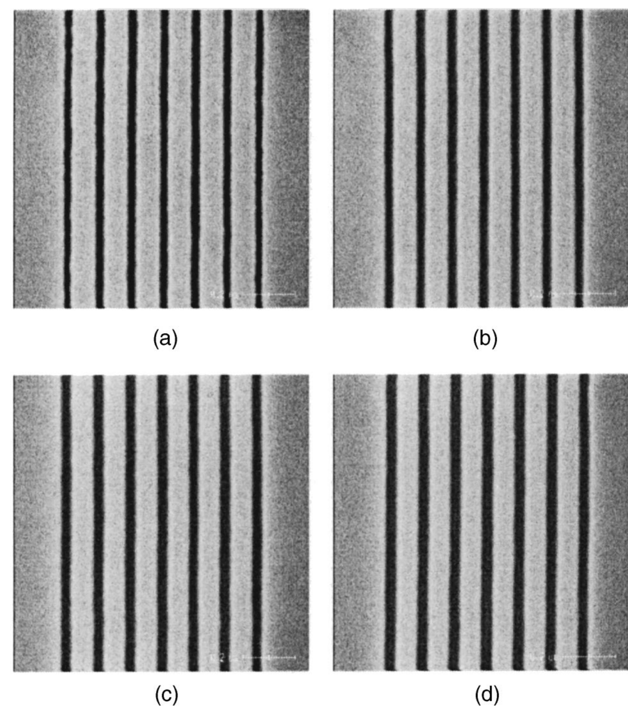

FIG. 5. SEM images of 40 nm spaces/80 nm lines on a completed SFIL template. CD measurements are: (a) 32.4 nm; (b) 32.9 nm; (c) 38.6 nm; and (d) 39.7 nm for process splits of 60%, 80%, 100%, and 120% Cr overtech. A 20 s descum was used.

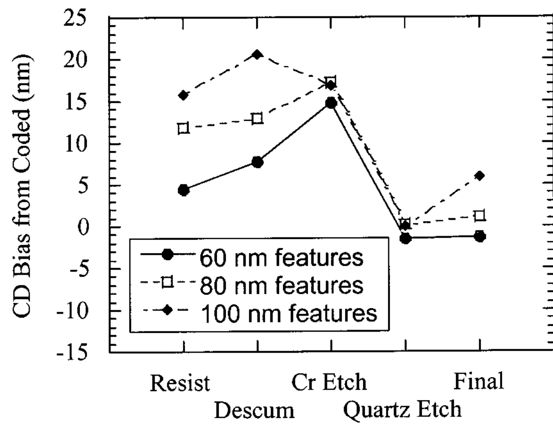

FIG. 6. Plot of CD bias from coded as a function of processing step.

C. Fabrication window

A 20 s descum coupled with a 110% Cr overetch was found to give the best performance in terms of CD control and line edge roughness. To a certain degree, increasing descum time could be used in conjunction with decreasing Cr overetch times to achieve comparable results. Thus, similar performance was observed for 40 s descum/80% Cr overetch and 60 s descum/60% Cr overetch combinations. This is not surprising since, in all three cases, total resist erosion is about 85 nm.

The overall typical trends observed for CD bias as a function of processing step used in the SFIL template fabrication process may be found in Fig. 6. Considering the data for 60 nm clustered features, the spaces are usually found to measure approximately 4 nm over coded size. The descum process increases CD by about the same magnitude, and resist erosion during Cr etch results in approximately 7 more nanometers of positive bias. After quartz etch, CD bias is 1.5 nm less than coded. As will be shown, the quartz sidewall angle is about 5° from the normal, and this fact, coupled with the threshold values on the SEM, most likely accounts for the large swing in CD. A separate internal study beyond the scope of the present work offers some corroboration of this hypothesis. The deeper the quartz etch, the smaller the measured CD. Over the quartz depth range of 50–150 nm, a negative 1 nm CD change is registered for every 6.5 nm depth increase. Moving back to the results of Fig. 6, final CD bias ends up approximately 1 nm from coded after the Cr hardmask is stripped.

IV. FEATURE PROFILE

An extensive study was conducted to ascertain the feasibility of using AFM to nondestructively determine sidewall profile and etch depth on SFIL templates. Figure 7 graphically compares the results obtained for four different tip types when imaging 150 nm trenches in quartz. Not surprisingly, the tip size and shape were found to significantly influence the data, particularly for the smaller features of the present study. For example, the standard AFM tip, which possesses a typical radius of 5–10 nm and exhibits a conical

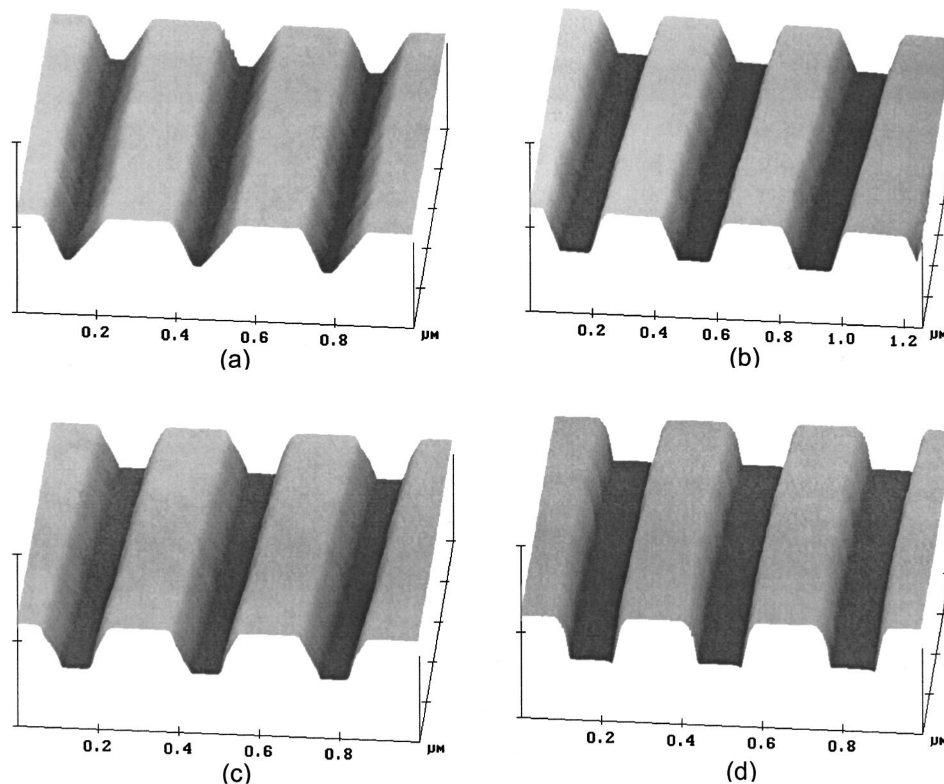

FIG. 7. AFM images of 150 nm spaces as imaged by various AFM tips: (a) standard; (b) carbon nanotube; (c) high aspect ratio; and (d) sharpened silicon. The effect of tip geometry is evident in the images.

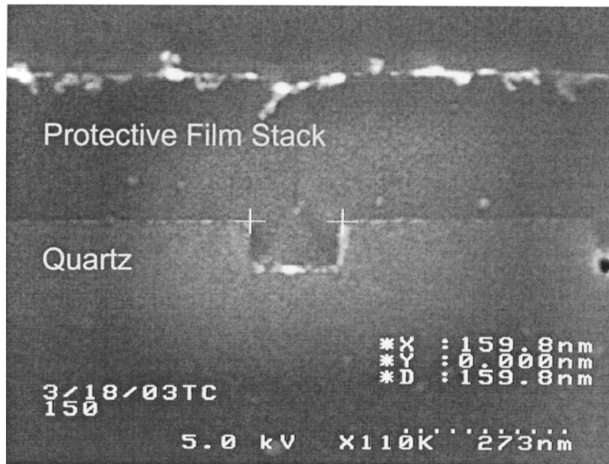

FIG. 8. Cross section of 150 nm trench on a 6025 plate. Preparation involved a FIB procedure and SEM imaging. The protective film stack for charge dissipation and sample protection is labeled.

cross section, was still able to fit into 150 nm trenches and determine etch depth with good accuracy. However, as will be shown, predicted sidewall angles of 118°–130° proved to be significantly different than actually present, with tip geometry as the underlying cause. When comparing standard, carbon nanotube, high aspect ratio, and sharpened silicon AFM tips, the sharpened silicon tips were able to measure 80 nm wide trenches nominally etched 100 nm deep into the quartz. Even with a 2 nm tip radius, geometrical considerations for the sharpened silicon tips limited sidewall angle determination to greater than 100°. In fact, as measured by these tips, sidewall angle and etch depth were found to be 102° and 89.6 nm, respectively.

Actual template cross sections are difficult to prepare and necessitate destruction of the part being analyzed, which, obviously, is not desirable. However, for the sake of obtaining direct evidence of feature sidewall angle and profile rather than inferring data from an imprint profile, a SFIL template was sacrificed and analyzed. An initial extensive manual polishing approach was unsuccessful due to material chipping. Polishing of an encapsulated sample was next attempted but also resulted in chipping. A viable approach for cross sectioning the trenches was found by using a focused ion beam tool. Due to extreme charging, sample drift, and surface damage associated with the sample material and the FIB technique, a protective film stack was deposited on the top surface of the sample. Following the FIB procedure, cross-sectional SEM analysis and measurements of the selected trench structures were obtained. Figure 8 contains a SEM image of a 150 nm trench prepared via the aforementioned technique. Using SEM measurements as a basis, sidewall angles of these features were calculated to be 94.8°. The analogous sidewall angle of larger 500 nm features was found to be almost identical, 95.6°. It is also interesting to note that the SEM measurements suggest an etch depth of 89.1 nm for the 150 nm features, and this number compares extremely well to AFM measurements described above.

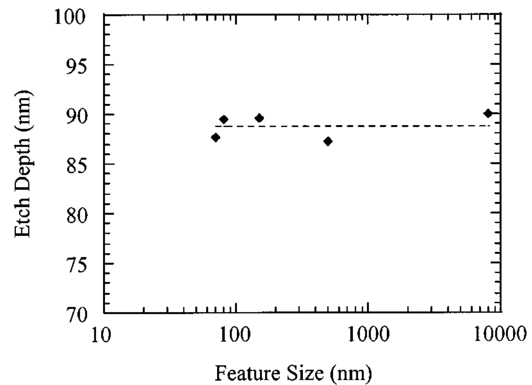

FIG. 9. Etch depth vs feature size as measured by AFM. Microloading effects are minimal down to the smallest feature size measured (70 nm).

V. MICROLOADING EFFECTS

Because no etch stop layer is present when etching the quartz substrate for SFIL template fabrication, the question of microloading becomes important. Variation in the etch depth into the quartz for different feature sizes will directly translate into different feature heights left behind on a wafer after the imprint process. Of course, this thickness variation would still exist on the wafer after the etch process was performed to remove the residual layer. In general terms, the precise shape and height of features cut into the etch barrier would then vary with feature size, and erosion of the etch barrier during the subsequent transfer layer etch could result in excessive CD loss that also varied with feature size. To avoid this would require the transfer layer etch process to have even higher selectivity of the ARC to the etch barrier material. Additionally, the thinner the etch barrier/ARC stack is, the more difficult it is to subsequently use the stack to pattern transfer an underlying dielectric or metal film for device fabrication.

Figure 9 contains a plot of quartz etch depth as a function of feature size as measured by AFM. It can be seen that the ICP process used to etch the quartz exhibits minimal microloading effects. Good linearity of etch depth was observed for all features sizes measured from 70 nm up to 8 μm. On the template analyzed, average feature depth was found to be 88.8 nm with a 1.2 nm variation (1 sigma). Trenches narrower than 70 nm could not be measured because of the aforementioned geometrical considerations related to the shape of the AFM probe tips. However, circumstantial evidence for smaller features is available from cross sections taken on imprinted wafers. SEM images of imprinted features as small as 30 nm suggest that microloading effects on the template are negligible. Data is not currently available below 30 nm. Further studies are planned in which broadband reflectometry and other techniques will be investigated to measure sub-100 nm features.

VI. CONCLUSION

SFIL potentially offers a low cost, high throughput alternative to other lithographies. We have demonstrated a physical masking process for generating dry etch process window

information quickly, yet without sample-to-sample variation. The combination of descum time and Cr overetch can be used to tailor critical dimensions by about 15 nm on SFIL masks in order to achieve coded line sizing or some other target. In terms of CD control and line edge roughness, the best performance was observed with a 20 s descum coupled with a 110% Cr overetch. Although geometrical considerations limited sidewall angle determination to greater than 100°, sharpened silicon AFM tips were able to measure 80 nm wide trenches nominally etched to a depth of 100 nm into the quartz substrates. Albeit destructive, a FIB technique was successfully demonstrated for cross-sectioning of features on a 6025 plate. Finally, the quartz etch process employed was shown to be essentially devoid of microloading effects over the range of 70 nm to 8 μm. Because SFIL technology could reasonably be expected to be implemented at feature sizes smaller than 50 nm, further studies are planned for nondestructive characterization of template properties at these smaller sizes.

ACKNOWLEDGMENTS

Fabrication of templates for this work was performed by the staff of Motorola Labs' Microelectronics and Physical Sciences Laboratory. In particular, Anne Dinsmore and Lester Casoose, both of Motorola's DigitalDNA™ Laboratories, are to be recognized for their tireless SEM inspection and metrology support. The authors would additionally like to thank Kevin Williamson and Troy Clare, also in Motorola's DigitalDNA™ Laboratories, for FIB preparation and SEM cross-sectional analysis on 6025 plates. Finally, it should be noted that this work was funded in part by DARPA N66001-01-1-8964.

[1]M. Colburn, S. Johnson, M. Stewart, S. Damle, T. Bailey, B. Choi, M. Wedlake, T. Michaelson, S. V. Sreenivasan, J. Ekerdt, and C. G. Willson, Proc. SPIE **3676**, 171 (1999).
[2]T. C. Bailey, D. J. Resnick, D. Mancini, K. J. Nordquist, W. J. Dauksher, E. Ainley, A. Talin, K. Gehoski, J. H. Baker, B. J. Choi, S. Johnson, M. Colburn, M. Meissl, S. V. Sreenivasan, J. G. Ekerdt, and C. G. Willson, Microelectron. Eng. **61/62**, 461 (2002).
[3]D. P. Mancini, K. A. Gehoski, W. J. Dauksher, K. J. Nordquist, D. J. Resnick, P. Schumaker, and I. McMackin, Proc. SPIE **5037**, 187 (2003).
[4]W. J. Dauksher, D. J. Resnick, S. B. Clemens, D. L. Standfast, Z. S. Masnyj, J. R. Wasson, N. M. Bergmann, S.-I. Han, and P. J. S. Mangat, J. Vac. Sci. Technol. B **18**, 3232 (2000).
[5]K. H. Smith, J. R. Wasson, P. J. S. Mangat, W. J. Dauksher, and D. J. Resnick, J. Vac. Sci. Technol. B **19**, 2906 (2001).